J. Fluid Mech. (1974), *vol.* 65, *part* 4, *pp.* 799–824
Printed in Great Britain

An oscillating-boundary-layer theory for ciliary propulsion

By C. BRENNEN
Engineering Science Department, California Institute of Technology, Pasadena

(Received 2 November 1973)

This paper analyses the locomotion of a finite body propelling itself through a viscous fluid by means of travelling harmonic motions of its surface. The methods are developed with application to the propulsion of ciliated micro-organisms in mind. Provided that the metachronal wavelength (of the surface motions) is much smaller than the overall dimensions of the body, the flow can be divided into an oscillating-boundary-layer flow to which is matched an external complementary Stokes flow. The present paper employs the envelope model of fluid/cilia interaction to construct equations of motion for the oscillating boundary layer. The final solution for the propulsive velocity is obtained by application of the condition of zero total force on the self-propelling body; alternatively, if the organism is held at rest, the thrust it generates can be computed. Various optimum propulsive velocities for self-propelling bodies and optimum thrusts for restrained bodies are analysed in some simple examples. The results are compared with the relatively sparse observations for a number of micro-organisms.

1. Introduction

The general fluid-mechanical problem studied in this paper is that of a body propelling itself through viscous fluid by means of small-amplitude harmonic motions of its surface. The Reynolds number of the motion is assumed to be small though precise definition of this condition is delayed until later. The frequency ω of the motions is assumed to be invariant over the surface of the body and with time. The predominant interest lies in surface disturbances in the form of waves travelling over the surface of the body. This theory is developed with one particular application in mind, namely, the propulsion of ciliated micro-organisms. A significant body of work now exists on the fluid dynamics of ciliary locomotion and in view of recent review articles by Jahn & Votta (1972) and Blake & Sleigh (1974) the fundamental aspects of this intriguing subject will not be repeated here.

The material presented is intended to rectify a deficiency in the existing theoretical analyses of ciliary propulsion. The great majority of the fluid-mechanical research beginning with the pioneering work of Taylor (1951) and continuing through that of Tuck (1968), Blake (1971*b*, 1972) and others has been confined to the analysis of geometrically simplified models involving

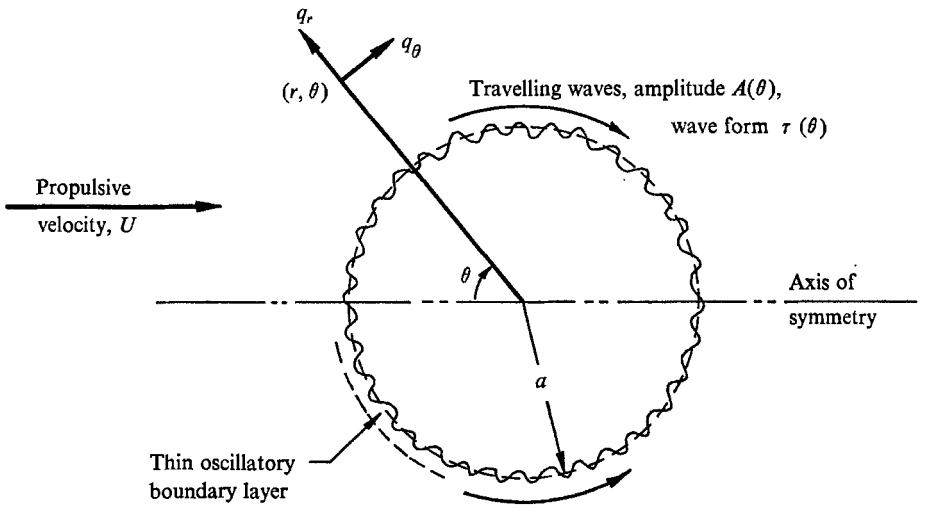

FIGURE 1. Schematic diagram illustrating the application of the oscillatory-boundary-layer technique.

flat sheets of infinite extent and infinitely long cylinders. The manner in which the results of such analyses should be applied to finite organisms, which are often ellipsoidal in shape, is not entirely obvious. The only finite-body analysis which appears in the literature is that of Lighthill (1952), later modified by Blake (1971*a*), who approximated the travelling surface waves on a sphere by combining two spherical harmonic functions whose orders differ by one. Such a solution is rather restrictive in terms of the permitted variation of the wave form and wave amplitude over the body and its extension to non-spheroidal bodies appears to involve considerable algebraic complexity.

The present paper takes a different approach to the general analysis of finite bodies by restricting attention to those organisms whose metachronal wavelength $2\pi/k$ is small compared with their overall dimensions. It follows that since the unsteady fluid motions generated by the cilia are generally attenuated like e^{-ky} with distance y from the surface (see below) the thickness of this layer is small compared with the body size. The overall flow around the organism (see figure 1) will thus be comprised of a thin oscillatory boundary layer outside which the flow is predominantly steady. Since the Reynolds numbers based on propulsive velocity and overall dimensions are extremely small for most organisms, the latter is termed the complementary Stokes flow. The basic idea will then be to match fluid-mechanical solutions obtained for the motions within the boundary layer to this complementary Stokes flow in order to predict the propulsive motions of the organism. In general such a procedure is independent of the particular means used to model the motions within the boundary layer. More specifically, in the case of ciliary propulsion such a technique is equally applicable to either of the existing models of fluid/cilia interaction, conveniently termed the envelope model and the sublayer model in the literature. These models, developed by Taylor (1951) and especially Blake (1971*a*, *b*, 1972), are

reviewed in Blake & Sleigh (1974). Both involve assumptions concerning the immediate interaction of the cilia and the fluid, assumptions which enable tractable fluid-mechanical models to be constructed. The present paper will use only the envelope model within the oscillatory boundary layer; it should however be appreciated that a similar analysis could be performed using a modified sublayer model.

Before embarking upon the construction of the solution, it is convenient to include some discussion of these interaction models. The envelope model assumes that the cilia are sufficiently closely packed together that the fluid effectively sees an oscillating material surface comprised of the tips of the cilia. This envelope is commonly assumed to be impenetrable and the locus of each material point on it may be determined from the locus of the tip of an individual cilium. Blake's (1972) sublayer model, on the other hand, considers the flow amongst the cilia; he calculates the interaction of the motion of an individual cilium with the parallel steady flow which the ciliary bed is assumed to create. The model, however, neglects the unsteady flow interactions between individual cilia. Blake & Sleigh (1974) argue that this model is more appropriate for cases in which the individual cilium tips are more widely spaced.

The two models are valid in different circumstances and it is important to establish some criterion for the boundaries of their validity. Clearly, the envelope model requires that the cilia totally entrain the fluid in the interstitial space so that the exterior fluid essentially experiences the motion of a flexible surface whose motions correspond roughly to those of the cilium tips. On the other hand, the sublayer model is valid only when the fluid entrained by an individual cilium does not interact significantly with neighbouring cilia.

Thus, one possible criterion which might be examined would compare the base separation d of the cilia (see figure 2) with the radius of the volume of fluid entrained by each cilium near its tip. Neglecting the presence of the nearby wall and neighbouring cilia this entrainment radius could be represented by the Stokes radius ν/q or $\nu/\omega L$, where q is a typical cilium velocity, ω is the radian frequency of beat, L is the cilium length and ν is the kinematic viscosity of the fluid. Thus we propose as a rough criterion that the envelope model becomes valid when $\nu/\omega L \geqslant d$. This must, however, be qualified by the effect of the nearby wall (see, for example, Blake 1971*c*). In a hypothetical situation in which ν is gradually increased, the influence of the wall will be felt as $\nu/\omega L$ becomes within an order of magnitude of L. But provided that $d/L \ll 1$ much of the interstitial fluid has already been entrained by this time. Values of $\nu/\omega L$ higher than d have little relevance except as an indication of maximum entrainment within the interstitial fluid. It therefore appears that the envelope model has considerable relevance provided that

$$\nu/\omega L \gg d, \quad d/L < 1. \tag{1}$$

A further qualification of these conditions is worth noting in view of Blake's (1972) observation that the actual ciliary separation during the effective stroke in antiplectic metachronism is much greater than d. A measure of this additional

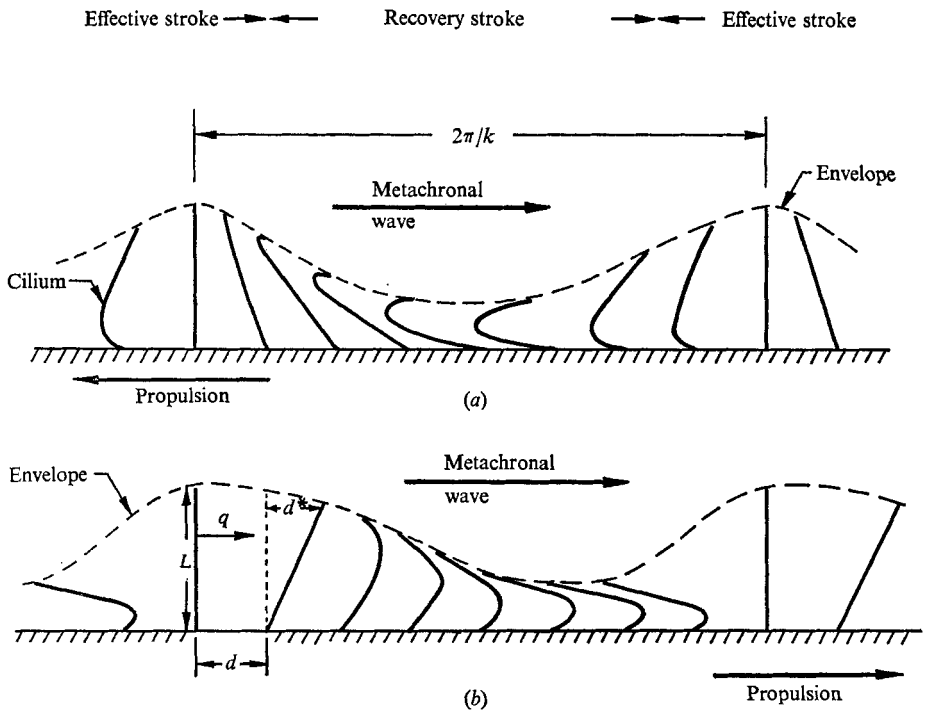

FIGURE 2. Schematic diagram of ciliary metachronism indicating the relative directions of metachronal wave propagation and propulsion of the body for (*a*) symplectic and (*b*) antiplectic metachronism. Note that during the effective stroke the direction of cilium motion is opposite to that of the propulsion. The equivalent material surface used in the envelope model is also shown.

cilium separation d^* is easily computed as kLd (figure 2), where $2\pi/k$ is the wavelength of the metachronal wave. Replacing d by d^* in the conditions (1) gives

$$\nu/\omega L \gg kLd, \quad kd < 1. \tag{2}$$

Taken together, conditions (1) and (2) should therefore define a fairly complete region of validity for the envelope model. Table 1 presents the values of these quantities for three organisms frequently used in locomotion studies. The data are taken from Sleigh (1962), Blake & Sleigh (1974), Knight-Jones (1954) and other sources. The values appear to confirm the validity of the envelope model for *Opalina* and reject it in the case of *Pleurobrachia*; *Paramecium* is a marginal case for which one would still expect some validity. Indeed a study of the conditions for other micro-organisms suggests that the envelope model may have wider validity than it has been given credit for in the literature.

2. Basic viscous flow formulation

In order to pave the way for the particular solutions of later sections, we shall begin by briefly outlining the equations and boundary conditions which govern the viscous flow induced by a material surface (or ciliary envelope) whose par-

Metachronism	*Opalina ranarum* Symplectic	*Paramecium* Dexioplectic	*Pleurobrachia* (figures given consider the comb-plates as the individual organelles) Normally antiplectic
Metachronal wavelength, $2\pi/k$ (μm)	25	10	7300
Cilium spacing, d (μm)	0·3–3·0	1·5–2·5	350
Cilium length, L (μm)	10–15	10–12	800
Frequency, $\omega/2\pi$ (Hz)	4	30–35	10
kL	2·5–4·0	6–7	0·7
Oscillatory Reynolds number, $W = \omega/k^2\nu$	0·0004	0·0005–0·0007	85
$\nu/\omega L$ (μm)	4000	500	20
kLd (μm)	0·7–10·0	9–18	240
kd	0·07–0·7	0·9–1·5	0·3

TABLE 1

ticles are performing small-amplitude oscillatory motions. The vector $\mathbf{z}_0$ will denote the mean position of the surface in a co-ordinate system which is fixed relative to the mean motion of the surface; thus $\mathbf{z}_0$ can also be considered to be the Lagrangian label for a particular surface particle whose position at time t is $\mathbf{z}_s$. This motion can be generally represented by

$$\mathbf{z}_s - \mathbf{z}_0 = \mathrm{Re}\{\mathbf{Z}(\mathbf{z}_0)\, e^{-i\omega t}\} + \ldots, \tag{3}$$

where t is time, Re denotes 'the real part of' and $\mathbf{Z}$ is a complex vector. Let the order of magnitude of Z be ϵ; further terms on the right-hand side such as higher harmonics will be assumed to be of order ϵ^2 or higher. The analysis will be confined to purely oscillatory surface motions so that ω is real. It follows that the velocity $\mathbf{q}_s$ of a surface particle is

$$\mathbf{q}_s = \omega\, \mathrm{Im}\{\mathbf{Z}\, e^{-i\omega t}\} + \ldots. \tag{4}$$

Now let the viscous flow of the fluid near the surface (and resulting in part from the movement of the surface) be represented by the velocity $\mathbf{q}(\mathbf{z})$. If the conditions of no slip and impenetrability of the surface are applied, it follows that a fluid element next to the surface has the same velocity as the surface particle with which it is in contact. Then the following Taylor expansion relates the fluid and surface motions:

$$\mathbf{q}_s(\mathbf{z}_s, t) = \mathbf{q}(\mathbf{z}_0, t) + [\{(\mathbf{z}_s - \mathbf{z}_0).\nabla\}\, \mathbf{q}(\mathbf{z}, t)]_0 + \ldots, \tag{5}$$

where ∇ is the gradient operator and terms with subscript zero are evaluated on the mean surface $\mathbf{z}_0$. The expressions (3) and (4) for $\mathbf{z}_s - \mathbf{z}_0$ and $\mathbf{q}_s$ can then be substituted into (5). Knowledge of the hydrodynamic solution will provide $\mathbf{q}$ and its spatial derivatives. Further, we propose a series solution to the Navier–Stokes equations (see below) for the fluid flow of the form

$$\mathbf{q} = \mathrm{Re}\,[\mathbf{q}_1\, e^{-i\omega t} + \{\mathbf{q}_2 + \mathbf{q}_3\, e^{-2i\omega t}\} + \ldots], \tag{6}$$

where $\mathbf{q}_1$, $\mathbf{q}_2$ and $\mathbf{q}_3$ are in general complex. It will be clear that a solution consistent with the foregoing boundary conditions will require q_1 to be of order ϵ and q_2 and q_3 to be of order ϵ^2; further terms in the series (6) will be of higher order. Thus (6) contains the first two terms in a series in ascending powers of ϵ. The function $\mathbf{q}_2(z)$ can be assumed purely real without loss of generality.

Thus substituting (3), (4) and (6) into (5) and equating coefficients of $\cos\omega t$ and of $\sin\omega t$ yields

$$-i\omega\mathbf{Z} = (\mathbf{q}_1)_0 + \{(\mathbf{Z}.\nabla)\,\mathbf{q}_2 + (\tfrac{1}{2}\bar{\mathbf{Z}}.\nabla)\,\mathbf{q}_3\}_0 + \ldots, \tag{7}$$

where an overbar denotes a complex conjugate. Terms independent of t give

$$(\mathbf{q}_2)_0 = -\tfrac{1}{4}[(\mathbf{Z}.\nabla)\,\bar{\mathbf{q}}_1 + (\bar{\mathbf{Z}}.\nabla)\,\mathbf{q}_1]_0 + \ldots \tag{8}$$

and coefficients of $\cos 2\omega t$ and $\sin 2\omega t$ yield

$$(\mathbf{q}_3)_0 = -[(\mathbf{Z}.\nabla)\,\mathbf{q}_1]_0 + \ldots. \tag{9}$$

Equation (7) demonstrates that q_1 must, in general, be of order ϵ; (8) and (9) declare q_2 and q_3 to be of order ϵ^2, so that the last term in the brackets in (7) is then of order ϵ^3. Further, the neglected terms in (6)–(9) are then respectively of order ϵ^3, ϵ^5, ϵ^4 and ϵ^4. Hence it follows that we may substitute the approximate version of (7), namely

$$\mathbf{Z} = i(\mathbf{q}_1)_0/\omega, \tag{10}$$

into (8) and (9) and still maintain the same order of accuracy in those equations (neglected terms being of order ϵ^4). The result is

$$(\mathbf{q}_2)_0 = -(i/4\omega)\,[(\mathbf{q}_1.\nabla)\,\bar{\mathbf{q}}_1 - (\bar{\mathbf{q}}_1.\nabla)\,\mathbf{q}_1]_0, \tag{11}$$

$$(\mathbf{q}_3)_0 = -(i/\omega)\,[(\mathbf{q}_1.\nabla)\,\mathbf{q}_1]_0. \tag{12}$$

Equation (11) represents the boundary condition on the steady component of the viscous flow. The quadratic combination on the right-hand side is the first of three nonlinear terms which play an essential role in determining the self-propulsion of the body. It arises simply from kinematic considerations on the oscillating boundary and has been previously identified by Blake (1971*b*) and others as the major propulsive effect in the envelope model of ciliary propulsion.

The Navier–Stokes equations for the flow of an incompressible Newtonian fluid are

$$\frac{D\mathbf{q}}{Dt} = \frac{\partial\mathbf{q}}{\partial t} + (\mathbf{q}.\nabla)\,\mathbf{q} = -\frac{\nabla p}{\rho} + \nu\nabla^2\mathbf{q}, \tag{13}$$

with the continuity equation $\nabla.\mathbf{q} = 0$. If the vorticity $\boldsymbol{\Omega}$ is defined in the normal way as $\boldsymbol{\Omega} = \nabla\times\mathbf{q}$ the equation for $\boldsymbol{\Omega}$ from (13) is

$$\partial\boldsymbol{\Omega}/\partial t - \nabla\times(\mathbf{q}\times\boldsymbol{\Omega}) = \nu\nabla^2\boldsymbol{\Omega}. \tag{14}$$

The vorticity $\boldsymbol{\Omega}$ will be expanded in a series similar to the series (6) for the velocity, so that

$$\boldsymbol{\Omega} = \mathrm{Re}\,[\boldsymbol{\Omega}_1 e^{-i\omega t} + \{\boldsymbol{\Omega}_2 + \boldsymbol{\Omega}_3 e^{-2i\omega t}\} + \ldots], \tag{15}$$

where $\boldsymbol{\Omega}_n = \nabla \times \mathbf{q}_n$, Ω_1 is $O(\epsilon)$ and Ω_2 and Ω_3 are $O(\epsilon^2)$. Substitution of (15) into (14) yields

$$\nabla^2 \boldsymbol{\Omega}_1 = -i\omega \boldsymbol{\Omega}_1/\nu + O(\epsilon^3), \tag{16}$$

$$\begin{aligned}\nabla^2 \boldsymbol{\Omega}_2 &= -(4\nu)^{-1}[(\bar{\boldsymbol{\Omega}}_1 . \nabla)\,\mathbf{q}_1 + (\boldsymbol{\Omega}_1 . \nabla)\,\bar{\mathbf{q}}_1 - (\mathbf{q}_1 . \nabla)\,\bar{\boldsymbol{\Omega}}_1 - (\bar{\mathbf{q}}_1 . \nabla)\,\boldsymbol{\Omega}_1] + O(\epsilon^4) \\ &= -(4\nu)^{-1}[\nabla \times (\mathbf{q}_1 \times \bar{\boldsymbol{\Omega}}_1) + \nabla \times (\bar{\mathbf{q}}_1 \times \boldsymbol{\Omega}_1)] + O(\epsilon^4).\end{aligned} \tag{17}$$

The right-hand side of (17) represents the second nonlinear contribution to the steady component of flow. However, because this arises from the convective inertial terms in the Navier–Stokes equations, its order of magnitude generally differs from that of the kinematic contribution by virtue of the Reynolds number W (represented by the factor $1/\nu$). Its influence is therefore slight at the typically small values of W relevant to ciliary propulsion.

The characteristics of the solution of the basic equations (16) and (17) with boundary conditions (10) and (11) are best illustrated by an example. Consider a body (micro-organism) propelling itself through a fluid otherwise at rest by means of an oscillating surface (ciliary field). Given the surface motion $\mathbf{Z}$ the oscillatory first-order fluid motion $\mathbf{q}_1$ may be found entirely from (16) and (10); the condition that the total energy imparted to the fluid by the body must be finite requires that $\mathbf{q}_1$ be rather rapidly attenuated with distance from the surface (usually like e^{-ky}, where k is the wavenumber and y is normal to the surface). It follows that the right-hand sides of the equation (17) for $\mathbf{q}_2$ and condition (11) are then known functions, and the solution for $\mathbf{q}_2$ may be obtained.

But now an essential feature of the solution becomes evident. Clearly one may arbitrarily add to $\mathbf{q}_2$ *any* steady Stokes flow which has zero velocity on the mean surface. This addition would violate none of the conditions or equations established thus far, yet would arbitrarily alter the uniform streaming velocity at infinity (or propulsive velocity). Clearly the missing element is the fundamental condition that the total force on the self-propelling body must be zero. Only after application of this condition can the propulsive velocity be calculated. In order to impose this condition the stresses on the oscillating material surface, whose fundamental development is included in the next section, must be evaluated.

For the mathematical analysis it is convenient to divide $\mathbf{q}_2$ into a particular solution $\mathbf{q}_2^p$ which obeys (11) but which involves *no* streaming motion at infinity and a complementary solution $\mathbf{q}_2^c$, referred to earlier as the complementary Stokes flow. The latter must therefore satisfy

$$\nabla^2 \mathbf{q}_2^c = 0 \tag{18}$$

and the boundary condition

$$(\mathbf{q}_2^c)_0 = (i/4\omega)\,[\nabla \times (\mathbf{q}_1 \times \bar{\mathbf{q}}_1)]_0 - (\mathbf{q}_2^p)_0. \tag{19}$$

After application of the zero-total-force condition, the uniform streaming $\mathbf{q}_2^c$ at infinity will yield the propulsive velocity of the body.

3. Stresses on the oscillating material surface

In this section the stresses on an element of oscillating material surface are analysed so that the condition of zero total force may be obtained by integration of these stresses over the entire surface of a body or organism. Within the fluid the stress tensor will be denoted by $\boldsymbol{\pi}$, where in the normal fashion

$$\boldsymbol{\pi} = -p\mathbf{I} + 2\mu\boldsymbol{\Delta},$$

p being the hydrostatic pressure, $\mathbf{I}$ the idemfactor and $\boldsymbol{\Delta}$ the rate-of-deformation tensor. Clearly both $\boldsymbol{\pi}$ and p may be expanded in the same manner as $\mathbf{q}$:

$$\boldsymbol{\pi} = \mathrm{Re}\,[\boldsymbol{\pi}_1 e^{-i\omega t} + \{\boldsymbol{\pi}_2 + \boldsymbol{\pi}_3 e^{-2i\omega t}\} + \ldots], \tag{20}$$

$$p = \mathrm{Re}\,[p_1 e^{-i\omega t} + \{p_2 + p_3 e^{-2i\omega t}\} + \ldots]. \tag{21}$$

Consider an element of oscillating surface and define orthogonal surface co-ordinates (s_1, s_2) and a normal co-ordinate y on the corresponding element of *mean* surface. If $\mathbf{l}$, $\mathbf{m}$ and $\mathbf{n}$ are unit vectors in the s_1, s_2 and y directions and Z_1, Z_2 and Z_3 are the components of $\mathbf{Z}$ in these three directions then a vector element $d\mathbf{S}_I$ of the instantaneous surface is related to the element $\mathbf{n}\,ds_1\,ds_2$ of mean surface by

$$\frac{d\mathbf{S}_I}{ds_1 ds_2} = \mathbf{n} + \mathrm{Re}\left[\left\{-\mathbf{l}\frac{\partial Z_3}{\partial s_1} - \mathbf{m}\frac{\partial Z_3}{\partial s_2} + \mathbf{n}\left(\frac{\partial Z_2}{\partial s_2} + \frac{\partial Z_1}{\partial s_1}\right)\right\} e^{-i\omega t}\right]. \tag{22}$$

Using (8) this may be written as

$$\frac{d\mathbf{S}_I}{ds_1 ds_2} = \mathbf{n} - \mathrm{Re}\left[\frac{i\,e^{-i\omega t}}{\omega}\nabla((\mathbf{q}_1)_0 . \mathbf{n})\right]. \tag{23}$$

Now the force on this element at any instant in time is given by $\boldsymbol{\pi}_I . d\mathbf{S}_I$, where the subscript I denotes evaluation at the instantaneous position in the fluid. Here $\boldsymbol{\pi}_I$ must be replaced by a quantity evaluated on the mean surface by expanding in Taylor series in the manner previously used for the surface boundary condition, i.e.

$$\boldsymbol{\pi}_I = \boldsymbol{\pi}_0 + \{(\mathbf{z}_s - \mathbf{z}_0) . \nabla)\,\boldsymbol{\pi}\}_0 + \ldots . \tag{24}$$

Using (23) and (24) we may evaluate the effective local force on the element $ds_1 ds_2$ of mean surface. This comprises oscillatory forces and steady forces arising from the nonlinearity in (24). When the steady component is extracted as being of particular interest and a stress vector $\boldsymbol{\tau}^s$ is defined as the steady part of $\boldsymbol{\pi}_I . d\mathbf{S}_1$ divided by $ds_1 ds_2$, one obtains

$$\boldsymbol{\tau}^s = (\boldsymbol{\pi}_2)_0 . \mathbf{n} + (i/4\omega)\,[\{(\mathbf{q}_1 . \nabla)\,\bar{\boldsymbol{\pi}}_1 - (\bar{\mathbf{q}}_1 . \nabla)\,\boldsymbol{\pi}_1\} . \mathbf{n} + \boldsymbol{\pi}_1 . \nabla(\bar{\mathbf{q}}_1 . \mathbf{n}) - \bar{\boldsymbol{\pi}}_1 . \nabla(\mathbf{q}_1 . \mathbf{n})]_0. \tag{25}$$

Thus a third quadratic combination of first-order oscillatory terms makes its appearance in the solution and contributes to the solution $\mathbf{q}_2$ for the steady flow. This third contribution arises from the expression for the stresses on the material surface and makes its contribution to the propulsive velocity through the condition of zero total force on the body. We shall see that for finite bodies this

contribution is generally of the same order of magnitude as that arising from the kinematic surface condition, a fact which does not appear to have been elucidated before. The oversight is probably due to the fact that this third contribution is identically zero in solutions for infinite plane sheets or cylinders, a feature of these simple analyses which is further discussed in the following section. It follows that to draw conclusions on the propulsive velocity of an organism on the basis of infinite models is to neglect totally this first-order contribution. As demonstrated by the examples of § 6, its effect may be to enhance or reduce the propulsive velocity of the body depending upon the nature of the surface motions or ciliary beat.

It is convenient to divide the stress $\boldsymbol{\tau}^s$ into a component $\boldsymbol{\tau}^p$ due to the particular solution $\mathbf{q}_2^p$ plus the additional quadratic component of (25), and a component $\boldsymbol{\tau}^c$ due entirely to the complementary Stokes flow. Hence

$$\boldsymbol{\tau}^p = [\boldsymbol{\pi}_2^p]_0 . \mathbf{n} + (i/4\omega)\,[\{(\mathbf{q}_1 . \nabla)\,\bar{\boldsymbol{\pi}}_1 - (\bar{\mathbf{q}}_1 . \nabla)\,\boldsymbol{\pi}_1\} . \mathbf{n} + \boldsymbol{\pi}_1 . \nabla(\bar{\mathbf{q}}_1 . \mathbf{n}) - \bar{\boldsymbol{\pi}}_1 . \nabla(\mathbf{q}_1 . \mathbf{n})]_0, \quad (26)$$

$$\boldsymbol{\tau}^c = [\boldsymbol{\pi}_2^c]_0 . \mathbf{n}, \quad (27)$$

where $\boldsymbol{\pi}_2^p$ and $\boldsymbol{\pi}_2^c$ arise from $\mathbf{q}_2^p$ and $\mathbf{q}_2^c$.

4. The infinite oscillating sheet

To prepare for the oscillating-boundary-layer theory of the following section, it is worth illustrating how the formulation of the preceding sections can be employed to solve the problem of a semi-infinite body of fluid bounded by an infinite sheet whose surface particles are performing small oscillations. This problem has been treated before, at least in part, by Taylor (1951), Tuck (1968) and Blake (1971*b*). Only the case in which the fluid motion is confined to an x, y plane perpendicular to the mean surface $y = 0$ is considered. The surface motion is comprised of waves travelling in the positive-x direction. Since the fluid flow is planar it is convenient to define stream functions ψ_1 and ψ_2^c corresponding to the velocity vectors $\mathbf{q}_1$ and $\mathbf{q}_2^c$. An appropriate solution to (16) is then

$$\psi_1 = \Gamma\{\sigma \exp(kix - ky) + \exp[kix + k(-\beta_1 + i\beta_2)\,y]\}. \quad (28)$$

In this expression k is the wavenumber of the surface motions and if W denotes the oscillatory Reynolds number $\omega/k^2\nu$, then

$$\beta_{1,2} = \{\tfrac{1}{2}[(1+W^2)^{\frac{1}{2}} \pm 1]\}^{\frac{1}{2}}. \quad (29)$$

Note that, when $W \ll 1$, $\beta_1 \approx 1 + \frac{1}{8}W^2$ and $\beta_2 \approx \frac{1}{2}W$. Further σ and Γ are arbitrary complex constants, which will shortly be replaced by constants having a more direct physical interpretation.

Substituting (28) into the right-hand side of (17) and integrating gives the particular solution ψ_2^p:

$$\psi_2^p = \frac{k^2\Gamma\bar{\Gamma}}{4\omega} W^2 \left[-\frac{\sigma}{(1+\beta_1+i\beta_2)^3} \exp[-k(1+\beta_1+i\beta_2)\,y] - \frac{\bar{\sigma}}{(1+\beta_1-i\beta_2)^3} \times \exp[-k(1+\beta_1-i\beta_2)\,y] - \frac{1}{4\beta_1^3} \exp(-2k\beta_1 y) \right]. \quad (30)$$

Note that this yields zero velocity as $y \to \infty$ in accordance with our requirement on ψ_2^v. The boundary conditions on ψ_2^c thus become [equation (19)]

$$(\partial\psi_2^c/\partial x)_0 = 0, \tag{31}$$

$$\left(\frac{\partial\psi_2^c}{\partial y}\right)_0 = -\frac{k^3\Gamma\bar{\Gamma}}{\omega}\left[\sigma\bar{\sigma} + \frac{(3\beta_1^2-1)}{2} + \sigma(\beta_1+i\beta_2) + \bar{\sigma}(\beta_1-i\beta_2)\right]$$

$$= +U, \text{ say.} \tag{32}$$

The appropriate complementary Stokes flow is thus simply $\psi_2^c = +Uy$. Hence, owing to its surface motions, the sheet is observed to swim through fluid otherwise at rest with a velocity $-U$ in the positive-x direction. The material surface motions are obtained through (10) as

$$x_s - x_0 = \mathrm{Re}\{(ik\Gamma/\omega)(-\beta_1+i\beta_2-\sigma)\exp[i(kx_0-\omega t)]\}, \tag{33}$$

$$y_s - y_0 = \mathrm{Re}\{(k\Gamma/\omega)(1+\sigma)\exp[i(kx_0-\omega t)]\}, \tag{34}$$

and clearly have a travelling wave form where (x_0, y_0) is the mean position of a surface particle ($y_0 = 0$) and (x_s, y_s) is its position at time t.

It is convenient to envisage these material surface motions as comprised of two travelling waves, one of displacement in a direction normal to the mean surface (the y wave) and one in the plane of that surface (the x wave). The motion can thus be characterized by three quantities, namely a basic amplitude, the ratio of the two amplitudes and a phase difference. In calculating these quantities from (33) and (34) it becomes clear that one should replace Γ and σ by one complex and one real parameter, τ and A respectively, which are more natural for the presentation of results:

$$(1+\tau) = 2(1+\sigma)/(1-\beta_1+i\beta_2), \quad A = (k^2/\omega)[\tfrac{1}{2}\Gamma\bar{\Gamma}\beta_1(\beta_1-1)]^{\frac{1}{2}}. \tag{35}$$

It follows that the propulsive velocity

$$U = -\frac{\omega}{k}A^2\left[\tau\bar{\tau} - \tau - \bar{\tau} - \frac{1}{\beta_1}\right] \tag{36}$$

is obtained from a surface motion whose amplitudes from (33) and (34) are

$$k^2|x_s-x_0|^2 = A^2(\tau-1)(\bar{\tau}-1), \tag{37}$$

$$k^2|y_s-y_0|^2 = A^2(\tau+1)(\bar{\tau}+1). \tag{38}$$

The real parameter A thus represents the basic amplitude of the surface motion; in later sections it is convenient to associate it with an 'equivalent' ciliary length l given by

$$l^2 = |x_s-x_0|^2 + |y_s-y_0|^2 = 2A^2(\tau\bar{\tau}+1)/k^2. \tag{39}$$

On the other hand the complex quantity τ contains information only on the ratio of the x- and y-wave amplitudes and the phase difference between them. For the purposes of visual presentation the quantity K will define the amplitude ratio, where from (37) and (38)

$$K = \frac{|x_s-x_0|^2 - |y_s-y_0|^2}{|x_s-x_0|^2 - |y_s-y_0|^2} = -\frac{(\tau+\bar{\tau})}{(1+\tau\bar{\tau})}. \tag{40}$$

Thus Taylor's (1951) first-order solution is the special case $K = -1$ of no tangential motion. On the other hand one of the cases treated by Tuck (1968) is that of

no normal motion, $K = +1$. Further, if the phase angle by which the x wave leads the y wave is denoted by $\theta_p - \frac{1}{2}\pi$ then

$$\tan\theta_p = \frac{i(\tau-\bar{\tau})}{(\tau\bar{\tau}-1)}, \quad \sin\theta_p = \frac{i(\tau-\bar{\tau})}{\{(\tau^2-1)(\bar{\tau}^2-1)\}^{\frac{1}{2}}}. \tag{41}$$

Thus the parameter τ defines both K, the amplitude-ratio parameter, and θ_p, the phase angle; indeed the inverse of (40) and (41) is

$$\tau = \frac{(1-K^2)^{\frac{1}{2}} - \cos\theta_p + iK\sin\theta_p}{K\cos\theta_p - i\sin\theta_p}. \tag{42}$$

This complex quantity τ will thus be termed the wave-form parameter. Each surface particle performs an elliptical orbit whose shape and orientation is easily related to and completely described by the two parameters K and θ_p or alternatively by the wave-form parameter τ. The variations are illustrated in figure 3, where the fluid should be envisaged as lying above a horizontal material surface whose fluctuations in position are travelling towards the right-hand side of the page. In the envelope model of ciliary motion these orbits may be considered as the loci of the cilium tips.

Other properties of the fluid motion are easily calculated. The rate $\dot{E}$ of dissipation of energy per unit area of the mean surface may be evaluated as

$$\dot{E} = (2\omega^2\mu/k)\,A^2[\tau\bar{\tau}+\beta_1], \tag{43}$$

μ being the dynamic viscosity. This is, of course, equal to the rate at which work is done by the surface on the fluid in producing the motion. Also of interest is the steady flux of fluid in the positive-x direction relative to the fluid at $y = \infty$. This flux per unit breadth of the planar flow is

$$\dot{M} = \frac{\omega A^2}{2k^2}\left[\tau\bar{\tau} + \frac{\beta_2(\beta_2+i)}{\beta_1(\beta_1+1)}\tau + \frac{\beta_2(\beta_2-i)}{\beta_1(\beta_1+1)}\bar{\tau} + \frac{(\beta_1^2+\beta_1-3)}{\beta_1^2}\right]. \tag{44}$$

The ratio $\dot{M}/U$ can then be considered as the displacement thickness of the oscillatory boundary layer.

Finally, it is particularly important to note, as Taylor (1951) did, that the mean stress on the oscillating surface must be zero from a simple momentum argument. Though further proof of this fact is unnecessary, it can be verified, albeit with considerable algebra, by substitution of the solution into (26) and (27). In this regard the reader is referred to equations (64) of the following section. It follows that this flat-sheet solution is somewhat degenerate in that the zero-total-force condition is automatically satisfied through the choice of the solution for ψ_2^c.

Two quantities of particular interest from the point of view of ciliary locomotion are the propulsive velocity for a given 'ciliary length' l and the propulsive velocity for a particular energy expenditure. From the above equations these ratios can be written in the alternative non-dimensional forms

$$\frac{U}{\omega kl^2} = -\frac{(\tau\bar{\tau}-\bar{\tau}-\tau-\beta_1^{-1})}{2(\tau\bar{\tau}+1)} = -\frac{1}{2}\left[\frac{(\beta_1-1)}{2\beta_1} + K - \frac{(\beta_1+1)}{2\beta_1}(1-K^2)^{\frac{1}{2}}\cos\theta_p\right], \tag{45}$$

$$\frac{\omega\mu U}{\dot{E}} = -\frac{(\tau\bar{\tau}-\bar{\tau}-\tau-\beta_1^{-1})}{2(\tau\bar{\tau}+\beta_1)} = -\left[\frac{\beta_1-1+2\beta_1 K-(\beta_1+1)(1-K^2)^{\frac{1}{2}}\cos\theta_p}{2\beta_1[(\beta_1+1)+(\beta_1-1)(1-K^2)^{\frac{1}{2}}\cos\theta_p]}\right]. \tag{46}$$

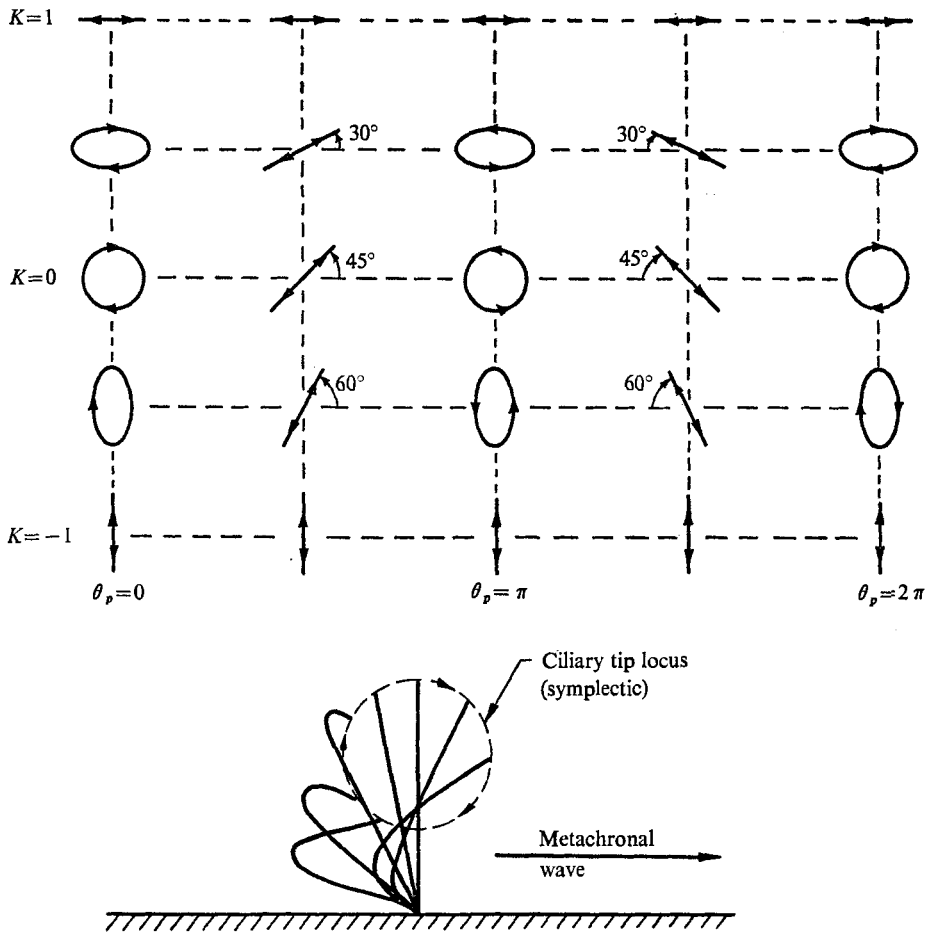

FIGURE 3. Diagram demonstrating how the elliptic locus of a surface particle varies with the parameters K and θ_p. Loci are shown for $K = -1$ to $+1$ in steps of 0·5 and for $\theta_p = 0$ to 2π in steps of $\frac{1}{2}\pi$. The mean surface is horizontal, the fluid above it and the surface waves travelling to the right. An example of a ciliary tip locus (symplectic) is indicated below.

In the limit $W \to 0$ of small Reynolds number both of these quantities are given simply by

$$U/\omega kl^2 \to \omega\mu U/\dot{E} \to \tfrac{1}{2}[(1-K^2)^{\frac{1}{2}}\cos\theta_p - K] \quad \text{as} \quad W \to 0. \tag{47}$$

This function is displayed graphically in figure 4. It is clearly seen that there are two modes of surface motion which yield optimal performances either in terms of the velocity for a given length l or in terms of the velocity for a given energy expenditure. In the case $K = -1/\sqrt{2}$ with $\theta_p = 0$ a maximum propulsive velocity of $U/\omega kl^2 = 1/\sqrt{2}$ is obtained in the *opposite* direction to the wave propagation, a situation which corresponds to symplectic metachronism in ciliary propulsion. The values $K = +1/\sqrt{2}$ and $\theta_p = \pi$ yield the same optimal velocity in the *same* direction as the wave propagation and hence correspond to optimum antiplectic ciliary motion.

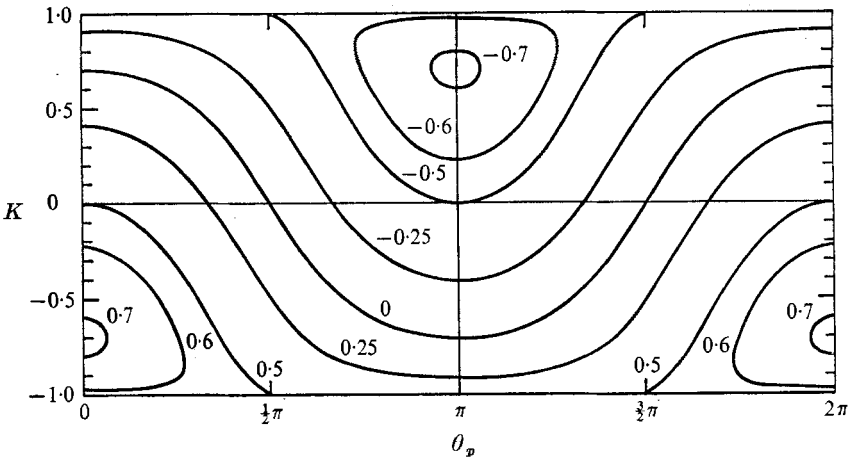

FIGURE 4. The variation of the propulsive velocity $U/\omega kl^2$ or $\omega\mu U/\dot{E}$ with wave-form type given by K and θ_p for the infinite-flat-sheet solution when $W \to 0$. Contours are labelled with values of $U/\omega kl^2$ or $\omega\mu U/\dot{E}$.

Similar figures were generated for finite W. However, even with $W = 1$, the results were negligibly different from those of figure 4, and since the validity for $W > 1$ is clearly in doubt no such figures are presented. Though the effect is extremely small and therefore probably not of any practical application, it is interesting to note that the effect of W on the optimum values of $U/\omega k^2 l$ is to reduce the absolute value of the symplectic optimum by $\frac{1}{64}(2+\sqrt{2})\,W^2$ while increasing the antiplectic optimum by $\frac{1}{64}(2-\sqrt{2})\,W^2$. But these values appear too small to justify any preference for antiplectic metachronism in micro-organisms.

Finally, it is readily demonstrated from the above relations that the mass flow in the positive-x direction relative to the fluid at infinity is given by

$$4\dot{M}/\omega l^2 \to -(1-K^2)^{\frac{1}{2}}\cos\theta_p \quad \text{as} \quad W \to 0. \tag{48}$$

Values of this quantity are identical to those shown in a later graph, figure 9. Note that the maxima are different from these of figure 4. It can also be shown that $\dot{M}$ is directly proportional to the area described by the ciliary loci of figure 3.

5. Oscillating-boundary-layer theory

Having developed the basic equations in §§ 2 and 3 and delineated the features of the infinite-sheet solution in the last section, we have laid the foundations for the development of governing equations for the oscillatory boundary layer on a finite body in accordance with the ideas outlined in the introduction. The basic approach will involve a generalization of the infinite-sheet solution so as to permit the wave form τ and amplitude A of the surface motions to be slowly varying functions of the position x on the mean surface. For this purpose the following generalized form of (28) is suitable:

$$\psi_1 = \Gamma[\sigma\, e^{\xi z} + e^{\eta z + \zeta x}], \tag{49}$$

where $z = k(x+iy)$ and Γ, σ, ξ, η and ζ are constants. The fact that this can only represent a planar or nearly planar local flow is a substantial approximation; it must therefore be noted that the solutions constructed will be inaccurate in the neighbourhood of stagnation points and other regions of rapidly diverging surface flow. Undoubtedly the solutions could be improved in this regard, but are developed in their present form for the sake of algebraic simplicity.

It follows by substitution into the equation of motion (16) that $\eta\zeta = -\frac{1}{4}iW$; we shall also define $\epsilon = \eta+\zeta-i$, where ϵ thus represents a deviation from the infinite-sheet solution of the last section, in which $\epsilon = 0$ and $\xi = i$. Then to order one in the small parameter ϵ

$$\eta = \tfrac{1}{2}\{\beta_2 + i(\beta_1+1)\} + \tfrac{1}{2}\epsilon[1+(\beta_1+i\beta_2)/(\beta_1^2+\beta_2^2)], \tag{50}$$

$$\zeta = \tfrac{1}{2}\{-\beta_2 + i(1-\beta_1)\} + \tfrac{1}{2}\epsilon[1-(\beta_1+i\beta_2)/(\beta_1^2+\beta_2^2)]. \tag{51}$$

Further, substitution of (49) into (10) reveals the nature of the travelling wave disturbances on a mean surface at $y = 0$. However, if we replace Γ and σ by $\tau(x)$ and $A(x)$, functions of x which are generalizations of the quantities employed in the last section and are defined by

$$\tau(x) = \{\sigma\xi \exp[k(\xi-i-\epsilon)x] + \eta\}/\zeta, \tag{52}$$

$$A(x) = (k^2/\omega)[\tfrac{1}{2}\Gamma\bar{\Gamma}\zeta\bar{\zeta}]^{\frac{1}{2}} e^{k\epsilon x}, \tag{53}$$

then the properties of the surface disturbance are given by precisely the same relations as in the last section, namely

$$k^2|x_s - x_0|^2 = A^2(\tau-1)(\bar{\tau}-1), \tag{54}$$

$$k^2|y_s - y_0|^2 = A^2(\tau+1)(\bar{\tau}+1), \tag{55}$$

$$K = -(\tau+\bar{\tau})/(1+\tau\bar{\tau}), \quad \tan\theta_p = i(\tau-\bar{\tau})/(\tau\bar{\tau}-1). \tag{56), (57}$$

The difference is that the amplitude $A(x)$ and the wave form $\tau(x)$ as well as K, θ_p, etc. are now permitted to be slowly varying functions of x through the introduction of the small parameters ϵ and $\xi-i-\epsilon$. However neither these parameters nor the expressions (52) and (53) will be explicitly calculated during the application of the equations developed here; they are merely introduced in order to permit $\tau(x)$ and $A(x)$ to be functions of x.

Equation (17) for the second-order steady motion can then be integrated to yield

$$\psi_2^p = -\frac{\Gamma\bar{\Gamma}k^2W^2}{32\omega}\left\{\frac{\sigma\xi}{(\xi+\bar{\xi})^2\bar{\eta}}\exp[(\xi+\bar{\xi})z+\bar{\eta}\bar{z}] + \frac{\bar{\sigma}\bar{\xi}}{(\bar{\xi}+\zeta)^2\eta}\exp[(\bar{\xi}+\zeta)\bar{z}+\eta z] + \frac{(2\eta\bar{\eta}-\zeta\bar{\zeta})}{(\eta+\bar{\xi})^2(\bar{\eta}+\zeta)^2}\exp[(\eta+\bar{\xi})z+(\bar{\eta}+\zeta)\bar{z}]\right\}. \tag{58}$$

From (11) the boundary conditions on the complementary solution become

$$\left(\frac{\partial\psi_2^c}{\partial x}\right)_0 = \left(\frac{\partial\phi}{\partial x}\right)_0, \quad \left(\frac{\partial\psi_2^c}{\partial y}\right)_0 = \left(\frac{\partial\phi}{\partial y}\right)_0, \tag{59}$$

where

$$\phi = \frac{\Gamma\bar{\Gamma}k^2}{2\omega}\left\{\sigma\bar{\sigma}\xi\bar{\xi}\exp(\xi z+\bar{\xi}\bar{z})+\sigma\xi\left\{\bar{\eta}+\frac{W^2}{16}\frac{1}{(\xi+\bar{\zeta})^2\bar{\eta}}\right\}\exp[(\xi+\bar{\zeta})z+\bar{\eta}\bar{z}]\right.$$
$$+\sigma\xi\left\{\eta+\frac{W^2}{16}\frac{1}{(\bar{\xi}+\zeta)^2\eta}\right\}\exp[(\bar{\xi}+\zeta)\bar{z}+\eta z]$$
$$\left.+(\zeta\bar{\zeta}-\eta\bar{\eta})\left\{1+\frac{W^2}{16}\frac{2}{(\eta+\bar{\zeta})^2(\bar{\eta}+\zeta)^2}\right\}\exp[(\eta+\bar{\zeta})z+(\bar{\eta}+\zeta)\bar{z}]\right\}. \quad (60)$$

By employing the parameters A and τ and expanding in the small parameters ϵ and $\xi-i-\epsilon$ these conditions are evaluated to leading order in the small parameters as

$$\left(\frac{\partial\psi_2^c}{\partial y}\right)_0 = q_t^c = -\frac{\omega A^2}{k}\Sigma_1, \quad \left(-\frac{\partial\psi_2^c}{\partial x}\right)_0 = q_n^c = \frac{\partial}{\partial x}\left(\frac{\omega A^2}{k^2}\Sigma_2\right), \quad (61)$$

where
$$\Sigma_1 = \tau\bar{\tau}-\tau-\bar{\tau}-\beta_1^{-1}, \quad (62)$$

$$\Sigma_2 = \frac{(\beta_1+5)}{2\beta_1^2}-\frac{1}{2}\left\{\tau+\frac{\beta_2(\beta_2-i)}{\beta_1(\beta_1+1)}\right\}\left\{\bar{\tau}+\frac{\beta_2(\beta_2+i)}{\beta_1(\beta_1+1)}\right\}. \quad (63)$$

Thus q_t^c and q_n^c represent the tangential and normal velocities at the mean surface required of the complementary Stokes flow; they are completely prescribed given the surface motions over the body, namely $A(x)$ and $\tau(x)$. Note especially that q_t^c is of zeroth order whereas q_n^c is of first order in the small parameters ϵ and $\xi-i-\epsilon$. This means that our expansion solution is valid only when the normal velocities q_n^c in the complementary solution are small compared with the tangential velocities q_t^c (see next section).

Finally, in order to implement the zero-total-force condition, the components of the surface stress must be evaluated. The surface stress $\boldsymbol{\tau}^p$ [equation (26)] will have components tangential and normal to the surface, denoted respectively by τ_t^p and τ_n^p. After substitution of the solution into (26) and considerable algebra these components can be evaluated to lowest order in the small parameters ϵ and $\xi-i-\epsilon$ as

$$\tau_t^p = \frac{\partial}{\partial x}\left(\frac{\rho\omega^2A^2}{k^3}\Sigma_3\right), \quad \tau_n^p = \frac{\partial}{\partial x}\left(\frac{\rho\omega^2A^2}{k^3}\Sigma_4\right), \quad (64)$$

where
$$\Sigma_3 = -\frac{1}{2}\left[\left(\tau+1+\frac{4i}{W}\right)\left(\bar{\tau}+1-\frac{4i}{W}\right)-\frac{8(\beta_1^2+1)}{W^2}\right], \quad (65)$$

$$\Sigma_4 = -\frac{1}{2}\left[\frac{4}{W}\left(\tau-\frac{iW}{4}\right)\left(\bar{\tau}+\frac{iW}{4}\right)-\frac{4\beta_1}{W}-\frac{W}{4}\right]. \quad (66)$$

A force $\mathbf{F}^p$ on the organism can then be obtained by integration of these stresses over the entire surface. Note that τ_t^p and τ_n^p become zero when both A and τ are constants; this is precisely what occurs in the infinite-sheet solution and confirms the much simpler momentum argument for that case. Consequently $\mathbf{F}^p$ is a function of the rate of change of the wave-form parameter and amplitude over the surface of the body. In addition, a force $\mathbf{F}^c$ due to the complementary Stokes flow may be obtained in the conventional manner by integration of $\boldsymbol{\tau}^c$ [equation (27)] over the surface. This will be a function not only of the boundary

conditions (61) on the complementary Stokes flow, but also of the unknown propulsive velocity U at infinity. Hence application of the zero-total-force condition $\mathbf{F}^p + \mathbf{F}^c = 0$ will yield a value for the propulsive velocity U. During this procedure, the four quantities Σ_1, Σ_2, Σ_3 and Σ_4 will be evaluated as functions of the wave form and hence its variation over the mean surface of the organism. By way of simplification it should be noted that as W becomes very small these have the following asymptotic behaviour:

$$\Sigma_1 \to \tau\bar{\tau} - \bar{\tau} - \tau - 1, \quad \Sigma_2 \to 3 - \tfrac{1}{2}\tau\bar{\tau}, \quad W\Sigma_3 \to -2i(\tau - \bar{\tau}), \quad W\Sigma_4 \to 2(1 - \tau\bar{\tau}). \tag{67}$$

The details of the boundary-layer approach to self-propulsion of an oscillating body (micro-organism) have thus been developed in this section. Given the amplitude A and form τ of the surface motion over the body one first computes the boundary conditions on the complementary Stokes flow from (61). The general Stokes flow obeying these boundary conditions and exhibiting an unknown propulsive velocity at infinity must then be constructed; for an arbitrarily shaped body this, of course, presents the major hurdle remaining in this approach. (In this regard the recent work of Blake & Chwang (1974; also private communication), Chwang & Wu (1974*a*, *b*) and others which enables construction of such solutions from distributions of fundamental singularities could be most useful.) The complementary Stokes flow and the force $\mathbf{F}^c$ are then entirely defined except for the velocity at infinity or propulsive velocity U. This is finally obtained by integration of $\boldsymbol{\tau}^p$ using (64)–(66) to obtain $\mathbf{F}^p$ and consequent application of the zero-total-force condition.

Some simple examples of the implementation of the boundary-layer technique will be presented in the next section.

6. Self-propulsion of a spherical body

In order to present some simple examples of the boundary-layer analysis of self-propulsion, a body whose mean surface shape is spherical is chosen because of the ease of construction of a complementary Stokes flow. This is indicated in figure 1, where our convention implies that the surface waves travel over the body in the direction of increasing θ. Further restricting the example to axisymmetric surface motions, let us examine several examples in which the complementary Stokes flow consists solely of the first-order spherical harmonic function, so that

$$\left.\begin{aligned} q_\theta &= [U - C(a/r)^3 + D(a/r)]\sin\theta, \\ q_r &= [-U - 2C(a/r)^3 - 2D(a/r)]\cos\theta, \end{aligned}\right\} \tag{68}$$

where C and D are constants to be determined and U is the velocity in the $\theta = \pi$ direction as $r \to \infty$ (or the propulsive velocity in the $\theta = 0$ direction under a Galilean transformation).

This complementary Stokes flow must then be matched to the oscillatory boundary-layer motions by means of the conditions (61); specifically

$$q_\theta|_{r=a} = [U - C + D]\sin\theta = q_t^c = -(\omega A^2/k)\,\Sigma_1, \tag{69}$$

$$q_r|_{r=a} = [-U - 2C - 2D]\cos\theta = q_n^c = d\{(\omega A^2/k^2 a)\,\Sigma_2\}/d\theta. \tag{70}$$

Given the amplitude $A(\theta)$ and wave form $\tau(\theta)$ of the surface motions, $\Sigma_1(\theta)$ and $\Sigma_2(\theta)$ may be evaluated from the relations (62) and (63) so as to provide two equations for U, C and D. In specific applications it is convenient to integrate (70) and use

$$[-U-2C-2D]\sin\theta = (\omega A^2/k^2a)\,\Sigma_2 + B, \tag{71}$$

where B is an arbitrary constant independent of θ. It is now time to recall the restriction of the last section that q_n^c must be small compared with q_t^c; on the other hand Σ_1 and Σ_2 are by definition generally of the same order of magnitude. Hence by comparison of (69) and (71) the restriction reduces simply to our original condition that ka be large, that is, that the wavelength be small compared with the overall dimension of the body.

The force F^c on the body in the $\theta = \pi$ direction due to the complementary Stokes flow (68) is well known, namely

$$F^c = -8\pi\rho\nu aD, \tag{72}$$

and this must be equal to $-F^p$; from the relations (64) the zero-total-force condition thus becomes

$$D = \int_0^\pi -\sin\theta\cos\theta\frac{\partial}{\partial\theta}\left\{\frac{\omega A^2 W\Sigma_4}{4k}\right\} + \sin^2\theta\frac{\partial}{\partial\theta}\left\{\frac{\omega A^2 W\Sigma_3}{4k}\right\} d\theta, \tag{73}$$

which in combination with (69) and (70) should allow solution for C, D and the propulsive velocity U. However, the particular choice of complementary Stokes flow for this and the following examples also implies certain functional restrictions on the choice of $A(\theta)$ and $\tau(\theta)$ as shown by (69), (70) and (73). It should be noted that these functional restrictions can clearly be removed by choosing a more general form for the complementary Stokes flow. The objective here is to keep the examples as simple as possible.

We shall examine first a particularly simple case in which the wave amplitude $A(\theta) = A^* \sin^2\theta$, $B = 0$ and the wave form τ is invariant over the surface of the body, so that the Σ's are independent of θ. Equations (69), (70) and (73) then become

$$U - C + D = -\omega A^{*2}\Sigma_1/k,$$

$$-U - 2C - 2D = (ka)^{-1}\omega A^{*2}\Sigma_2/k,$$

$$D = -\omega A^{*2} W\Sigma_4/6k$$

and the solution yields the propulsive velocity U as

$$U = -\frac{2\omega A^{*2}}{3k}\left[\Sigma_1 + \frac{\Sigma_2}{2ka} - \frac{W\Sigma_4}{3}\right]. \tag{74}$$

Because the present method is restricted to large ka, the term Σ_2/ka may be neglected compared with Σ_1 and $W\Sigma_4$. With regard to these other terms, it is clear that the propulsive velocity which one might predict on the basis of an infinite-sheet model would contain simply the term Σ_1. As indicated earlier, one of the features of finite bodies which this paper has brought to light is the importance of the zero-total-force condition; the latter has contributed the term

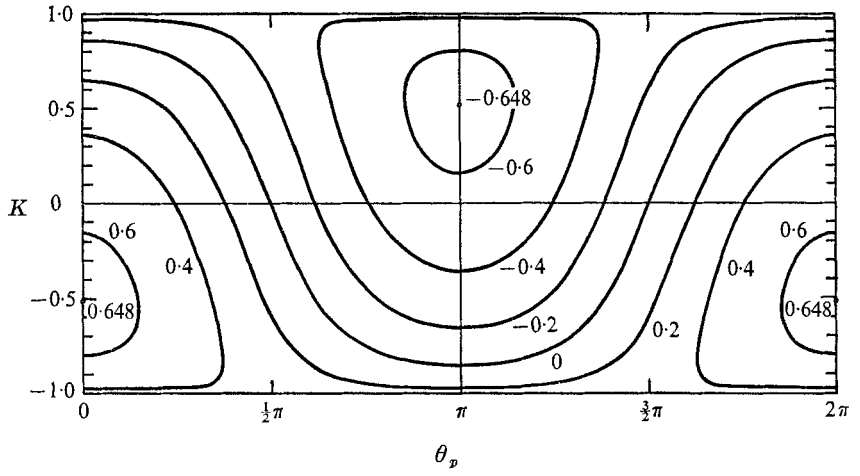

FIGURE 5. Variation of the propulsive velocity $U/\omega kl^2$ with wave form for the constant wave-form/varying amplitude example of the locomotion of a spherical body.

$W\Sigma_4$, which equations (67) indicate to be of the same order as Σ_1. Indeed for $W \ll 1$ those equations yield

$$U = (2\omega A^{*2}/3k)[1+\tau+\bar{\tau}-\tau\bar{\tau}+\tfrac{2}{3}(1-\tau\bar{\tau})]. \tag{75}$$

Further, by replacing A^* by an equivalent cilium length l at $\theta = \frac{1}{2}\pi$ according to the relation (39) this may be written in the alternative forms

$$U = \frac{kl^2\omega}{9}\left[\frac{5(1-\tau\bar{\tau})+3(\tau+\bar{\tau})}{1+\tau\bar{\tau}}\right] = \frac{kl^2\omega}{9}[5(1-K^2)^{\frac{1}{2}}\cos\theta_p - 3K] \tag{76}$$

using (56), (57) and (42). Values of $U/k\omega l^2$ are plotted in figure 5 as functions of the wave-form parameters K and θ_p. The figure therefore presents the propulsive velocity for this first example, in which the equivalent cilium length varies over the body like $l\sin^{\frac{1}{2}}\theta$ and in which the wave form, given by K and θ_p, is invariant over the surface. Optimum antiplectic propulsion, for which $U = -0{\cdot}648k\omega l^2$, occurs at $K = 3/\sqrt{34}$, $\theta_p = \pi$ while optimum symplectic propulsion, with $U = 0{\cdot}648k\omega l^2$, occurs at $K = -3/\sqrt{34}$, $\theta_p = 0$. Note that if one compares the corresponding infinite-model prediction evaluated by omitting the $W\Sigma_4$ term then the corresponding optima are $U = \mp 0{\cdot}472k\omega l^2$ at $K = \pm 1/\sqrt{2}$, $\theta_p = \pi, 0$. Hence the finite-body analysis actually predicts larger optimum propulsive velocities, though the optima occur with somewhat different wave forms.

In the foregoing first example the equivalent cilium length varied over the surface while the wave form remained constant. We shall now proceed to a second example, in which the equivalent cilium length l (or $A^2(1+\tau\bar{\tau})$) remains constant while the wave form varies over the surface in such a way as to produce the correct matching with the selected complementary Stokes flow (68). This situation is probably more realistic than the first example from the point of view of ciliary propulsion. If the analysis is simplified by restricting the investigation

to the case $W \ll 1$ and employing the relations (67) then it is readily established from (69) and (70) that the wave form $\tau(\theta)$ must be such that

$$(1+\tau+\bar{\tau}-\tau\bar{\tau})/(\tau\bar{\tau}+1) = E\sin\theta, \quad \text{where} \quad E = 2(U-C+D)/k\omega l^2,$$

and

$$(3-\tfrac{1}{2}\tau\bar{\tau})/(\tau\bar{\tau}+1) = F\sin\theta+G, \quad \text{where} \quad F = 2(-U-2C-2D)\,ka/k\omega l^2$$

and G is an arbitrary constant. If $W\Sigma_3$ and $W\Sigma_4$ are evaluated from these expressions for τ the zero-total-force condition becomes

$$D = -\tfrac{2}{21}\omega k l^2 F. \tag{77}$$

Hence by eliminating C and D the propulsive velocity U is found to be

$$U = \tfrac{1}{3}\omega k l^2[E+\tfrac{8}{21}F - F/ka]. \tag{78}$$

If τ_0 and τ_1, respectively, denote the wave-form parameters at $\theta = 0$ and $\frac{1}{2}\pi$ it follows that

$$E = (1+\tau_1+\bar{\tau}_1-\tau_1\bar{\tau}_1)/(1+\tau_1\bar{\tau}_1),$$

$$G = (3-\tfrac{1}{2}\tau_0\bar{\tau}_0)/(1+\tau_0\bar{\tau}_0),$$

$$F = (3-\tfrac{1}{2}\tau_1\bar{\tau}_1)/(1+\tau_1\bar{\tau}_1) - G,$$

with the restriction that $1+\tau_0+\bar{\tau}_0-\tau_0\bar{\tau}_0 = 0$. It is convenient for display purposes to replace τ_0 and τ_1 by similarly subscripted values K_0 and θ_{p0}, and K_1 and θ_{p1} describing the wave forms at $\theta = 0$ (or π) and $\theta = \frac{1}{2}\pi$. It follows from the above and relations (56), (57) and (42) that K and θ_p must vary over the surface like

$$K = K_1\sin\theta + (1-\sin\theta)\,K_0,$$

$$\tan\theta_p = \left[\frac{1-K^2}{\{\cos\theta_{p1}(1-K_1^2)^{\frac{1}{2}}\sin\theta+\cos\theta_{p0}(1-K_0^2)^{\frac{1}{2}}(1-\sin\theta)\}^2}-1\right]^{\frac{1}{2}}.$$

The restriction on τ_0 requires that

$$K_0 = (1-K_0^2)^{\frac{1}{2}}\cos\theta_{p0}. \tag{79}$$

Hence, as we trace out the variation of the wave form over the surface on a K, θ_p chart, the locus must begin on the solid line in figure 6. A number of different loci with different K_0, θ_{p0}, K_1 and θ_{p1} are shown as examples in that figure.

If the terms involving $1/ka$ are neglected the propulsive velocity (78) can then be written as

$$U = \tfrac{1}{9}\omega k l^2[-3K_1-2K_0+5\cos\theta_{p1}(1-K_1^2)^{\frac{1}{2}}]. \tag{80}$$

Optimum propulsion clearly occurs when K_0 takes its maximum or minimum value within the restriction (79). Hence the first step in the optimization is to set $K_0 = 1/\sqrt{2}$ and $\theta_{p0} = 0$ for antiplectic motion or $K_0 = -1/\sqrt{2}$ and $\theta_{p0} = \pi$ for symplectic motion. For the antiplectic case the resulting variation with K_1 and θ_{p1} is as illustrated in figure 7. (The corresponding symplectic figure merely requires changing the sign of K, U and $\cos\theta_p$.) The maximum negative or antiplectic propulsive velocity then occurs when

$$K_0 = 1/\sqrt{2}, \quad \theta_{p0} = 0, \quad K_1 = 3/\sqrt{34}, \quad \theta_{p1} = \pi,$$

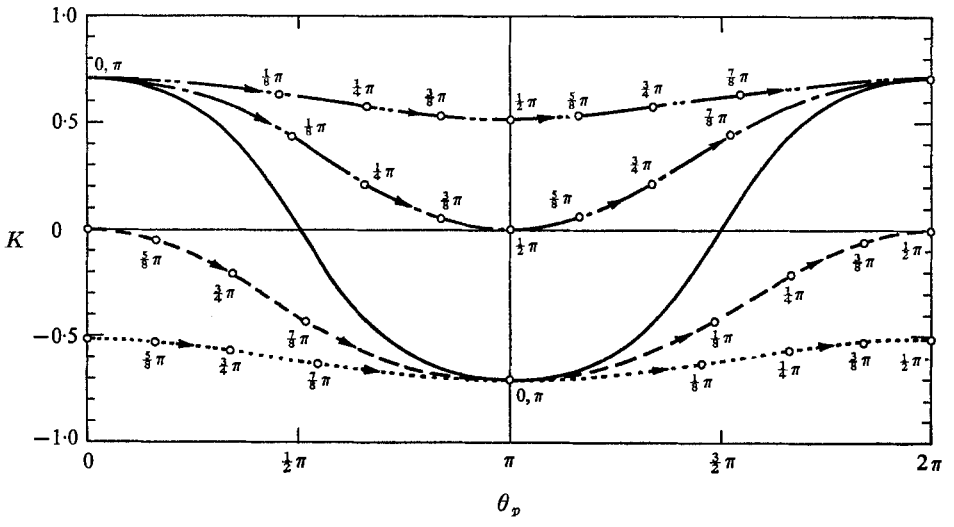

FIGURE 6. Examples of the variation in wave form over the surface for the case of a spherical body with constant equivalent cilium length and varying wave-form propulsion. ——, wave form at $\theta = 0, \pi$; ·····, locus for optimum symplectic propulsion; —·—, locus for optimum antiplectic propulsion; – – –, locus for optimum thrust of a restrained body in the direction of symplectic motion; —·—, locus for optimum thrust of a restrained body in the direction of antiplectic motion; ⊙, positions θ on the surface as shown; all loci are reversible in the sense that the indicated θ values may be replaced by $\pi - \theta$ and the direction of progression reversed.

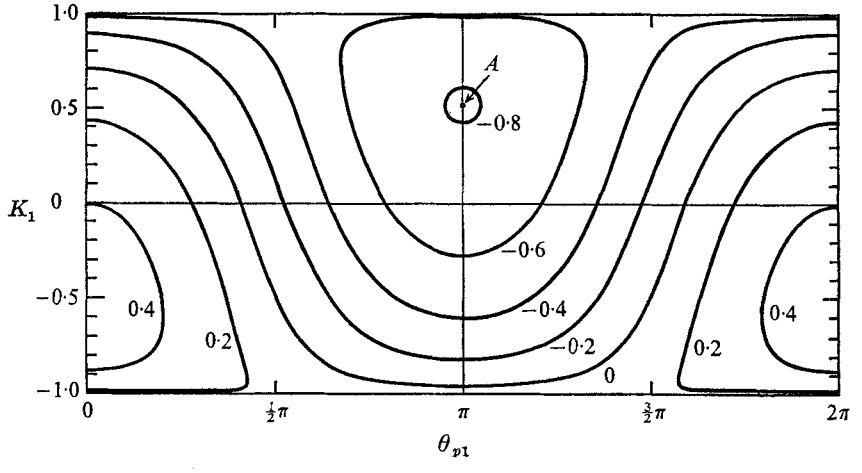

FIGURE 7. Variation of the propulsive velocity $U/k\omega l^2$ for a spherical body with constant equivalent cilium length and varying wave-form propulsion as a function of K_1 and θ_{p1} for fixed values of $K_0 = 1/\sqrt{2}$ and $\theta_{p0} = 0$. The latter values represent a partial optimization towards the maximum antiplectic motion. The final optimization in this regard is indicated by the point A.

while maximum positive or symplectic motion requires

$$K_0 = -1/\sqrt{2}, \quad \theta_{p0} = \pi, \quad K_1 = -3/\sqrt{34}, \quad \theta_{p1} = 0.$$

The wave-form variation over the surface for each of these cases is plotted in figure 6. In either case the velocity is

$$\{|U|/k\omega l^2\}_{\max} = \tfrac{1}{9}(\sqrt{2}+\sqrt{34}) = 0{\cdot}805.$$

Thus in this second example, which seems more realistic than the first as far as ciliary propulsion is concerned, the enhancement of propulsive velocity over that suggested by infinite models is even more significant.

The enhancement of the propulsive effect on the finite body may initially appear puzzling; one thinks of the added drag of the finite body and suspects a propulsive velocity less than that obtained by application of infinite-model results. A closer look with the help of the present examples reveals the inadequacy of such thoughts. It transpires that in the neighbourhood of optimum performance the sign of D is such that the force F^c due to the complementary Stokes flow does indeed represent a drag. But, in the first example, the variation of the wave amplitude and, in the second example, the variation of the wave form over the surface create a thrust which, in a sense, is more than adequate to balance this drag. Thus the propulsive velocity is enhanced over that suggested by the infinite models, simply so that the forces on the body or organism will balance. It does not follow that such enhancement will occur for all choices of variation of the wave form and amplitude over the surface but the effect is a significant one in the examples presented.

7. Comparison with observed propulsive velocities

It is worth attempting to compare the typical theoretical results with those from observations of different organisms even though such comparisons are hindered by the wide scatter in the experimental values quoted in the literature. Table 2 represents a distillation and assimilation of results from many different sources. The data on *Opalina ranarum* represent a typical example of the difficulties in that Sleigh's (1962) values of 1–4 Hz for the frequency and 100–200 μm/s for the metachronal wave speed seem inconsistent with the wavelengths of 5–25 μm which are clearly present in the micrographs of Tamm & Horridge (1970). The values in table 2 represent a reasonable compromise. The data on *Paramecium* are taken from Sleigh (1962, chap. 5), Parducz (1966), Jahn & Bovee (1967), Machemer (1972), Tamm (1972) and Winet (1973); those for *Tetrahymena* from Preston (1972) and Winet (1973); those for *Pleurobrachia* from Sleigh (1963, 1966) and Tamm (1973). The values quoted for K and θ_p were derived from the ciliary beat patterns described by Gray (1928), Knight-Jones (1954), Sleigh (1962, chap. 4) and others including the above references. More recently the beat patterns of some ciliates have been found on closer inspection to be strongly three-dmensional (e.g. Kuznicki, Jahn & Fonseca 1970). Nevertheless the derived values of K and θ_p for *Paramecium*, *Tetrahymena* and *Pleurobrachia* indicate that these organisms operate close to the

Organism	Body length (μm)	Cilium length L (μm)	From beat pattern: $\frac{l}{L}$	From beat pattern: K	From beat pattern: θ_p	Beat frequency $\omega/2\pi$ (Hz)	Metachronal wavelength $2\pi/k$ (μm)	Metachronal wave velocity $c = \omega/k$ (μm/s)	kl	Measured propulsive velocity U (μm/s)	$\frac{U}{c}$
Opalina ranarum	350	10–15	0·5	$\sim -0{\cdot}3$	$\sim \frac{3}{2}\pi$	4	25	100	1·2–1·8	50–100	0·5–1·0
Paramecium caudatum	220	10	0·8	$\sim 0{\cdot}76$	$\sim \pi$	28	10	280	5	800–1200	2·8–4·3
Paramecium multimicronucleatum	250	10	0·8	$\sim 0{\cdot}76$	$\sim \pi$	30	10–27	300–810	2–5	1170	1·45–3·9
Tetrahymena pyriformis	50	5–8	0·8	$\sim 0{\cdot}75$	$\sim \pi$	20	16	320	1·6–2·5	360–600	1·1–1·9
Pleurobrachia (Ctenophore)	15000	800	0·8	$\sim 0{\cdot}75$	$\sim \pi$	10	7300	73000	0·55	–	—

TABLE 2

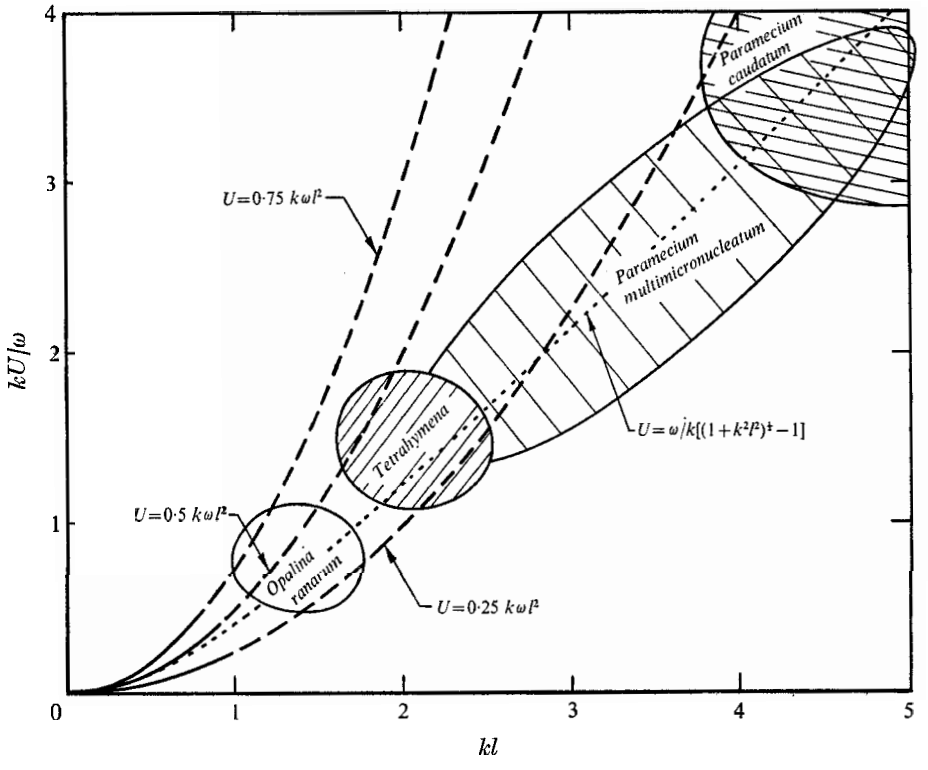

FIGURE 8. Non-dimensional propulsive velocity kU/ω as a function of the wave amplitude kl with observations from a number of ciliated micro-organisms (see table 2).

antiplectic optima demonstrated in figures 4, 5, 7 and 9; on the other hand *Opalina* clearly operates in the symplectic region.

A comparison of the propulsive velocities displayed in figure 8 must take into careful consideration the fact that the theory is limited to cases of small amplitude and could only be considered valid up to about $kl \approx \frac{1}{2}$. A reduction in the predicted propulsive velocity at greater amplitudes seems likely. Indeed the form of the basic equations involved in a nonlinear envelope-model analysis strongly suggests that the factor $\frac{1}{2}k^2l^2$ in the expression for the propulsive velocity is the linearized equivalent of $(1+k^2l^2)^{\frac{1}{2}}-1$. Though the details of this analysis will not be included here the latter function is plotted in figure 8 because of its significant correlation with observations. Finally it should be noted than an improvement in the quality of the observational data would considerably aid evaluation of various theoretical models.

8. Thrust on restrained organisms

The question of whether the ciliary motion of a particular micro-organism has evolved in such a way as to produce optimal motion does not lie within the scope of this paper. It is however useful to identify the wave forms or types of

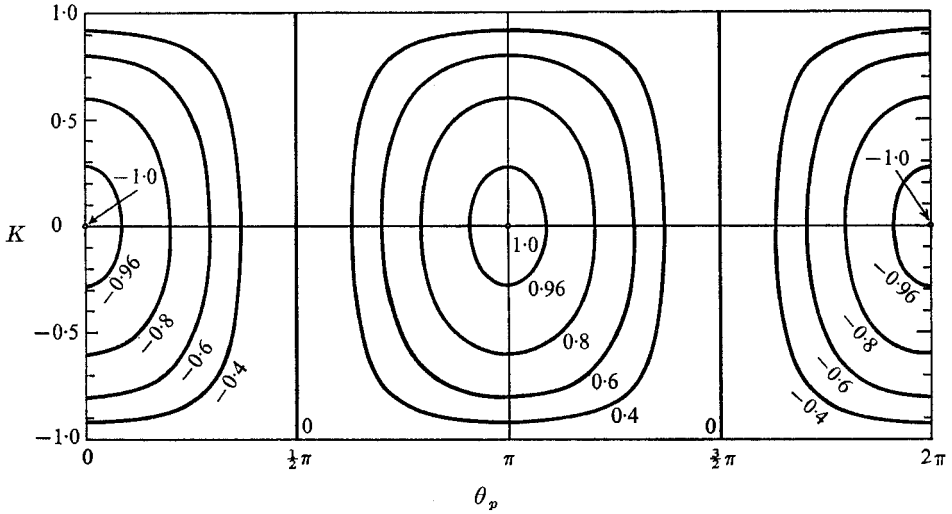

FIGURE 9. Variation of the generated thrust $3T/4\pi\mu\omega kal^2$ for a restrained spherical body exhibiting a constant wave-form and varying amplitude surface motion. (Note that precisely the same figure is relevant to the quantity $4\dot{M}/\omega l^2$ in the infinite-flat-sheet solution.)

ciliary motion which yield optimal performance within the limitations of the examples discussed. In this regard it should be noted that maximum rectilinear propulsive velocity may *not* be the most desirable and critical feature from the point of view of the organism. Clearly the ability to manoeuvre and accelerate may be of equal or greater importance. A trivial modification of the results of the examples in the last section permits study of the thrust that the organism can create if it is held at rest by an extraneous agent; this thrust will be some measure of the acceleration from rest which it could achieve if it were not restrained. If U is set equal to zero, the now finite thrust T in the $\theta = 0$ direction for the first example becomes

$$T = \tfrac{4}{3}\pi\mu\omega kal^2[(1-K^2)^{\frac{1}{2}}\cos\theta_p].$$

This is displayed in figure 9, which illustrates that the maximum thrust for symplectic motion occurs when $K = 0$ and $\theta_p = 0$ while that for antiplectic motion occurs at $K = 0$, $\theta_p = \pi$; the absolute value of the thrust is $\frac{4}{3}\pi\mu\omega kal^2$ in both cases. Approximate calculations using a mass plus added mass of $2\pi\rho a^3$ and the data of tables 1 and 2 indicate that the maximum initial accelerations for *Opalina* and *Paramecium* should be of order 1·5 and 100 body lengths/s^2 respectively. Accelerations of these orders of magnitude are consistent with observation.

In the second example of § 6, in which the wave form varies over the surface, the thrust on the restrained body or organism is

$$T = \tfrac{16}{21}\pi\mu\omega kal^2F = \tfrac{4}{3}\pi\mu\omega kal^2[\cos\theta_{p1}(1-K_1^2)^{\frac{1}{2}} - K_0].$$

Hence the maximum thrust for symplectic motion (positive T) is obtained when

$$K_0 = -1/\sqrt{2}, \quad \theta_{p0} = \pi, \quad K_1 = 0, \quad \theta_{p1} = 0,$$

while the optimum for antiplectic motion occurs when

$$K_0 = 1/\sqrt{2}, \quad \theta_{p0} = 0, \quad K_1 = 0, \quad \theta_{p1} = \pi.$$

These surface wave-form variations are also plotted in figure 8. They are significantly though not radically different from the corresponding wave-form variations for optimal rectilinear velocity. The optimal thrust in this case is somewhat larger than that generated in the first example, being $1 + 1/\sqrt{2}$ times greater.

9. Concluding remarks

In conclusion, this paper has presented a basic method for the fluid-mechanical analysis of the locomotion of ciliated micro-organisms. Provided that the metachronal wavelength is much smaller than the overall dimensions of the body, the flow can be divided into an oscillatory boundary-layer flow to which is matched an external complementary Stokes flow. The present analysis used the envelope model of fluid/cilia interaction to construct equations of motion for the oscillatory boundary layer. The final solution for the propulsive velocity is obtained by application of the condition of zero total force on the organism; alternatively, if the organism is held at rest, the thrust it generates can be computed.

Further analyses employing this basic method might use a different fluid/cilia interaction model, such as the sublayer model of Blake (1972). The present method could also be improved and extended by including cases in which the surface or ciliary-tip motion is three-dimensional and in which the direction of wave propagation differs from that of the effective stroke.

The author deeply appreciates the advice and encouragement of Professor T. Y. Wu and many suggestions and discussions with Dr John Blake, Dr Allen Chwang and Dr Howard Winet. This research was sponsored by the National Science Foundation under grant GK-31161X and by the Office of Naval Research under contract N00014-67-A-0094-0012.

REFERENCES

BLAKE, J. R. 1971*a* A spherical envelope approach to ciliary propulsion. *J. Fluid Mech.* **46**, 199–208.

BLAKE, J. R. 1971*b* Infinite models for ciliary propulsion. *J. Fluid Mech.* **49**, 209–222.

BLAKE, J. R. 1971*c* A note on the image system for a stokeslet in a no-slip boundary. *Proc. Camb. Phil. Soc.* **70**, 303–310.

BLAKE, J. R. 1972 A model for the micro-structure in ciliated organisms. *J. Fluid Mech.* **55**, 1–23.

BLAKE, J. R. & CHWANG, A. T. 1974 Fundamental singularities of viscous flow. Part I. The image systems in the vicinity of a stationary no-slip boundary. *J. Engng Math.* **8**, 23–29.

BLAKE, J. R. & SLEIGH, M. A. 1974 Mechanics of ciliary locomotion. *Biol. Rev.* **49**, 85–125.

CHWANG, A. T. & WU, T. Y. 1974*a* Hydromechanics of low-Reynolds-number flow. Part 1. Rotation of axisymmetric prolate bodies. *J. Fluid Mech.* **63**, 607–622.

CHWANG, A. T. & WU, T. Y. 1974*b* Hydromechanics of low-Reynolds-number flow. Part 2. Translation of spheroids; the nature of Stokes paradox. *J. Fluid Mech.* (in press).

GRAY, J. 1928 *Ciliary Movement.* Cambridge University Press.

JAHN, T. L. & BOVEE, E. C. 1967 Motile behavior in protozoa. In *Research in Protozoology*, vol. 1. Pergamon.

JAHN, T. L. & VOTTA, J. J. 1972 Locomotion of protozoa. *Ann. Rev. Fluid Mech.* **4**, 93–116.

KNIGHT-JONES, E. W. 1954 Relations between metachronism and the direction of ciliary beat in Metazoa. *Quart. J. Micro. Sci.* **95**, 503–521.

KUZNICKI, L., JAHN, T. L. & FONESCA, J. R. 1970 Helical nature of the ciliary beat of *Paramecium multimicronucleatum*. *J. Protozool.* **17**, 16–24.

LIGHTHILL, M. J. 1952 On the squirming motion of nearly spherical deformable bodies through liquids at very low Reynolds numbers. *Comm. Pure Appl. Math.* **5**, 109–118.

MACHEMER, H. 1972 Temperature influences on ciliary beat and metachronal coordination in *Paramecium*. *J. Mechanochem. Cell Motility*, **1**, 57–66.

PARDUCZ, B. 1966 Ciliary movement and coordination in ciliates. *Int. Rev. Cytol.* **21**, 91–128.

PRESTON, J. T. 1972 Determination of a continuous helical ciliary beat in *Tetrahymena pyriformis* and the cytotic effect of serum complement from normal and cystic fibrotic sera on the organism. Ph.D. thesis, University of California, Los Angeles.

SLEIGH, M. A. 1962 *The Biology of Cilia and Flagella.* Pergamon.

SLEIGH, M. A. 1963 Movements and coordination of the ciliary combplates of the ctenophores *Beroe* and *Pleurobrachia*. *Nature*, **199**, 620–000.

SLEIGH, M. A. 1966 Some aspects of the comparative physiology of cilia. *Am. Rev. Respiratory Diseases*, **93**, 16–31.

TAMM, S. L. 1972 Ciliary motion in *Paramecium*. A scanning electron microscope study. *J. Cell. Biol.* **55**, 250–255.

TAMM, S. L. 1973 Mechanisms of ciliary coordination in ctenophores. *J. Exp. Biol.* **59**, 231–246.

TAMM, S. L. & HORRIDGE, G. A. 1970 The relation between the orientation of the central fibrils and the direction of beat in cilia of *Opalina*. *Proc. Roy. Soc.* B**175**, 219–233.

TAYLOR, G. I. 1951 Analysis of the swimming of microscopic organisms. *Proc. Roy. Soc.* A**209**, 447–461.

TUCK, E. O. 1968 A note on a swimming problem. *J. Fluid Mech.* **31**, 305–308.

WINET, H. 1973 Wall drag on free-moving ciliated microorganisms. *J. Exp. Biol.* **59**, 753–766.